Comparison of the Structure of vMIP-II with Eotaxin-1, RANTES, and MCP-3 Suggests a Unique Mechanism for CCR3 Activation[†,‡]

Elias J. Fernandez,[§] Jill Wilken,[||] Darren A. Thompson,[||] Stephen C. Peiper,[⊥] and Elias Lolis*[,§]

Department of Pharmacology, Yale University School of Medicine, New Haven, Connecticut 06520, Gryphon Sciences, 250 East Grand Avenue, Suite 90, South San Francisco, California 94080, and Henry Vogt Cancer Research Institute, University of Louisville School of Medicine, Louisville, Kentucky 40404

Received May 23, 2000; Revised Manuscript Received July 17, 2000

ABSTRACT: Herpesvirus-8 macrophage inflammatory protein-II (vMIP-II) binds a uniquely wide spectrum of chemokine receptors. We report the X-ray structure of vMIP-II determined to 2.1 Å resolution. Like RANTES, vMIP-II crystallizes as a dimer and displays the conventional chemokine tertiary fold. We have compared the surface topology and electrostatic potential of vMIP-II to those of eotaxin-1, RANTES, and MCP-3, three CCR3 physiological agonists with known three-dimensional structures. Surface epitopes identified on RANTES to be involved in binding to CCR3 are mimicked on the eotaxin-1 and MCP-3 surface. However, the surface topology of vMIP-II in these regions is markedly different. The results presented here indicate that the structural basis for interaction with the chemokine receptor CCR3 by vMIP-II is different from that for the physiological agonists eotaxin-1, RANTES, and MCP-3. These differences on vMIP-II may be a consequence of its broad-range receptor recognition capabilities.

Kaposi's sarcoma-associated herpesvirus (KSHV)[1] contains three open reading frames that encode proteins with four positionally conserved cysteine residues that define the chemokine superfamily (*1*). One of these proteins, vMIP-II, is most closely related to human MIP-1α, MIP-1*β*, and RANTES at the level of primary structure (*2*). vMIP-II has been found to bind a uniquely broad spectrum of human G protein-coupled chemokine receptors, including members of the CC (CCR1, CCR2b, CCR3, CCR5, and CCR8), CXC (CXCR4), C (XCR1), and CX3C (CX3CR1) receptor subfamilies (*2*−*7*). This represents a unique feature of vMIP-II, as chemokines encoded by mammalian genes exclusively bind subsets of receptors within only one subfamily. The interaction of vMIP-II with CCR3 results in signal transduction (*2*). There have been conflicting reports describing in detail vMIP-II interactions with CCR8; both agonist (*5*) and antagonist activity (*8*, *9*) have been observed. vMIP-II behaves as an antagonist with the remainder of the above-mentioned receptors (*2*, *3*, *7*).

Since Kaposi's sarcoma is the most common malignancy in the acquired immunodeficiency syndrome (AIDS), both human immunodeficiency virus type 1 (HIV-1) and KSHV infection may coexist (*10*). The finding that patients with this neoplasm have reduced AIDS-related dementia or other central nervous system (CNS) manifestations of infection raises the possibility that KSHV may encode products that block the pathogenesis of the CNS damage induced by HIV-1 (*11*, *12*). The mechanism for this protection may involve inhibition of entry into target cells of the CNS, antagonism of viral infection within this compartment, or inhibition of toxicity to neural cells that is mediated by the HIV envelope protein (gp120) (*13*−*16*). As similar correlations have not been made for other herpesviruses, which may also cause infections during the course of AIDS, it is logical to consider neuroprotective candidates among ORFs unique to KSHV. Indeed, the binding of vMIP-II to the two major HIV coreceptors CCR5 and CXCR4 enables it to inhibit binding of gp120 from a variety of strains of HIV-1 and block infection in vitro (*2*, *3*). Some of the other chemokine receptors to which vMIP-II binds, particularly CCR2, CCR3, CCR8, and CX_3CR1 (*2*−*5*), have also been observed to function as HIV-1 coreceptors in vitro (*17*, *18*). This makes vMIP-II a strong candidate for neuroprotection.

The four positionally conserved cysteine residues of chemokines form intrachain disulfide bonds that stabilize these small proinflammatory proteins. Structural analysis reveals a highly conserved topology for each polypeptide that includes a flexible N-terminal segment that precedes the first cysteine, a long loop (the N-loop), three *β*-strands that form an antiparallel *β*-sheet, and a C-terminal α-helix. Amino acid residues critical for receptor binding and signaling were first localized to the N-terminal region (the N-loop and the unstructured N-terminus) of IL-8 (*19*−*21*) and have also been identified in the corresponding region of all chemokines subsequently studied, including RANTES (*22*), MCP-1 (*23*), MCP-2 (*24*), MCP-3 (*25*), eotaxin-1 (*26*), eotaxin-2 (*27*), MIP-2 (*28*), platelet factor-4 (*29*), MDC (*30*), and SDF-1α

[†] This work was supported by NIH Grant AI 43838 (E.L.).

[‡] Coordinates have been deposited in the Brookhaven Protein Data Bank under accession code 1CM9.

* To whom correspondence should be addressed: Department of Pharmacology, Yale University School of Medicine, New Haven, CT 06520. Telephone: (203) 785-6233. Fax: (203) 785-7670. E-mail: elias.lolis@yale.edu.

[§] Yale University School of Medicine.

[||] Gryphon Sciences.

[⊥] University of Louisville School of Medicine.

[1] Abbreviations: vMIP-II, viral macrophage inflammatory protein-II; RANTES, regulated upon activation, normal T-cell-expressed, and presumably secreted; MCP-3, monocyte chemoattractant protein-3; CCR3, CC chemokine receptor 3; KSHV, Kaposi's sarcoma-associated herpesvirus.

10.1021/bi001166f CCC: $19.00
Published on Web 09/26/2000

(*31*). In many cases, hybrid chemokines generated by the exchange of N-loops resulted in receptor binding and signaling properties defined by the N-loop sequences (*31*−*35*). It has therefore been concluded that the remainder of the protein serves as a scaffold to support the presentation of the N-loop and the N-terminus for interaction with receptors.

The unique biological properties of vMIP-II that have been demonstrated to date (i.e., its uniquely wide range of chemokine receptor engagement) and its potential protective role during HIV-1 infection make it an attractive target for understanding mechanisms of binding to this family of receptors. This information may elucidate approaches to the design of broadly acting inhibitors of inflammation and HIV-1 infection using vMIP-II as a template. We have previously used NMR to determine the secondary structure of vMIP-II and to investigate the dynamics of the unstructured region at the N-terminus (*36*, *37*). In the study presented here, we report the 2.1 Å X-ray crystal structure of vMIP-II and compare its molecular surface with three other chemokines that activate CCR3.

EXPERIMENTAL PROCEDURES

Chemical Synthesis and Crystallization of vMIP-II. For the X-ray crystallographic studies, vMIP-II and selenomethionine-modified vMIP-II (replacing Met-66) were synthesized, purified, and crystallized as described previously (*36*). The amino acid sequence corresponds to residues 21−94 of vMIP-II (GenBank accession number U75698). The protein was synthesized by thioester-mediated native chemical ligation of unprotected peptide fragments (*38*). Peptide segments were synthesized by solid-phase methods either manually or on an Applied Biosystems 430A peptide synthesizer. The polypeptide vMIP-II[(1−74)(−$SH)_4$] was purified and folded in 2 M guanidine HCl and 100 mM Tris (pH 8) containing 8 mM cysteine and 1 mM cystine. Met-66 was replaced with a selenomethionine residue for anomalous diffraction data collection. *N*-α-Fmoc-seleno-L-methionine was prepared from seleno-L-methionine (Sigma) and incorporated qualitatively into the peptide chain preactivated as the 1-hydroxy-7-azobenzotriazole ester. The resulting native and selenomethionine proteins were purified by reverse-phase HPLC and lyophilized.

Crystallization was initially achieved by the hanging-drop method. For X-ray diffraction data collection, vMIP-II, at a concentration of 10 mg/mL, was crystallized by the dialysis method (*39*). Crystals were obtained from 11% (w/v) polyethylene glycol 4000, 11% (v/v) 2-propanol, and 0.1 M citrate (pH 5.6).

Structure Determination. The structure was determined by multiwavelength anomalous diffraction (MAD) with three wavelengths collected from a single crystal using the inverse beam method at beamline X4C of the National Synchrotron Light Source at Brookhaven National Laboratory (Upton, NY) (Table 1). Difference Patterson maps using data from the remote wavelength and at maximum dispersion confirmed the positions of the two selenium atoms using the PHASES program package (*40*). Initial phases were calculated by SOLVE (*41*) to 3.0 Å resolution. Phases were improved further by solvent flattening and histogram matching using DM (*42*, *43*). A distinct solvent boundary encompassing small stretches of secondary structure could be observed around the two molecules in the asymmetric unit. Short stretches of polyalanine residues were built into similar regions of the two molecules. Phases were further improved by 2-fold averaging using DMMULTI (*42*, *43*) from an initial matrix calculated using LSQMAN (*42*, *43*). The above process of updating and refining the 2-fold relationship between the two molecules was carried out for several cycles. Initial MAD phases were also calculated using all data to 2.1 Å using SHARP (*44*). The SHARP maps were used along with the density-modified maps from SOLVE to place side chain atoms into density.

Table 1: Crystallographic and Refinement Statistics for vMIP-II

wavelength (Å)	0.9793 (12 660 eV)	0.9790 (12 664 eV)	0.9871 (12 560 eV)
scattering factors (e^-)			
f'/f''	−9.4/3.3	−7.4/5.3	−4.79/0.532
resolution limit (Å)	30−2.1	30−2.1	30−2.1
no. of unique reflections	8210	8251	8259
completeness (%)	92.9	92.7	92.8
overall R_{sym} (%)[a]	8.3 (38.1)	7.3 (43.8)	6.4 (46.0)
refinement statistics			
resolution range (Å)	30−2.1		
R_{free}/R_{cryst} (%)	27.5/24.1		
rms deviations			
bond lengths (Å)	0.007		
bond angles (deg)	1.311		

[a] The numbers in parentheses are from the outer resolution shell (2.2−2.1 Å).

Model Building, Refinement, and Analysis. Refinement of the model was performed using the maximum likelihood protocol as incorporated in CNS (*45*). Hendrickson−Lattman coefficients from the initial phased set were used throughout the refinement. The model was built into electron density using the program O (*46*). Initially, refinement was performed using strict noncrystallographic symmetry. Toward the end of the refinement process, the two molecules in the asymmetric unit were refined separately. The structure was analyzed graphically using the INSIGHT software package (Molecular Simulations Inc.). Superposition of vMIP-II and the chemokines eotaxin-1, RANTES, and MCP-3 was also performed with the INSIGHT program package. Coordinates for eotaxin-1 (PDB code 1EOT), RANTES (PDB code 1RTO), and MCP-3 (PDB code 1BO0) were obtained from the Protein Data Bank. The electrostatic surface potential maps were generated using the DelPhi program (*47*) as incorporated in the INSIGHT program package.

RESULTS

Structure Determination and Description. The structure of vMIP-II was determined to 2.1 Å by multiwavelength anomalous diffraction using a chemically synthesized selenomethionine protein (Table 1). The structure was refined to an *R*-free value of 27.5% and an *R*-factor of 24.0% for the reflections between 30.0 and 2.1 Å. The final model consists of residues 7−74 (molecule A), residues 8−74 (molecule B), and 22 water molecules. All residues are in the allowed region of the Ramachandran plot. The overall rms difference between the two molecules based on the Cα atoms is 0.58 Å. An example of the electron density is displayed as a $2F_o - F_c$ map in Figure 1. The N- and C-terminal residues appear to be flexible, as no electron

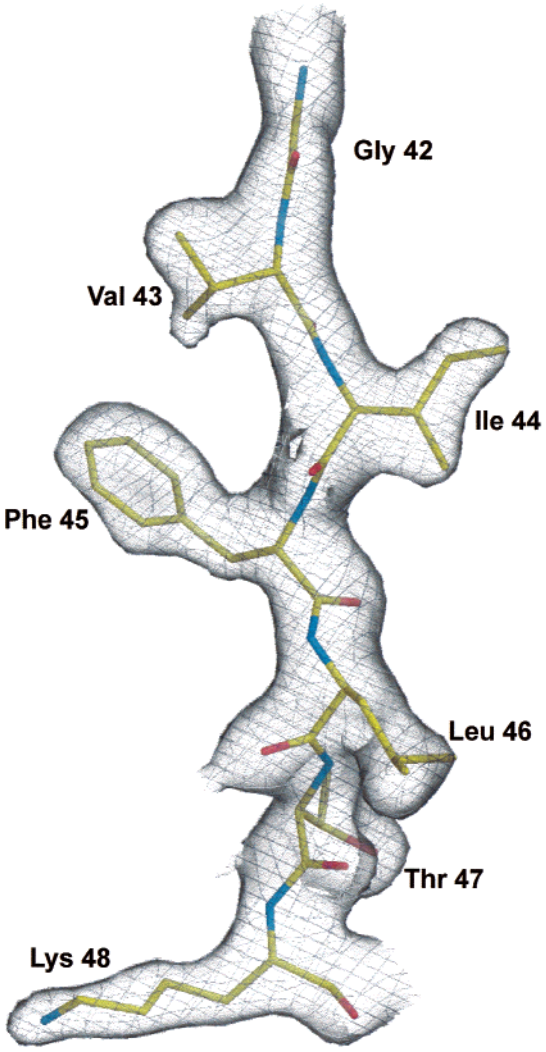

FIGURE 1: Final $2F_o - F_c$ map superimposed on residues 42−48. This figure was produced with the programs BOBSCRIPT (*69*, *72*) and Raster3D (*70*).

density is present. Figure 2A shows an α-carbon trace for the vMIP-II monomer. The monomer displays an α/*β* topology with three *β*-strands forming an antiparallel *β*-sheet. The C-terminal α-helix packs against the *β*-sheet. As with other CC chemokines, this motif is stabilized by two disulfide bonds and a conserved hydrophobic core. These residues include the four cysteines (Cys-14, Cys-15, Cys-38, and Cys-54), Leu-23, Leu-28, Trp-31, Val-43, Ile-44, Phe-45, Val-53, Ala-55, Trp-61, Val-62, Leu-65, Met-66, and Leu-69.

In contrast to solution studies with vMIP-II, which indicate that vMIP-II is a monomer at millimolar concentrations and at various pHs and NaCl concentrations (*36*, *37*), the asymmetric unit of the crystal contains an elongated dimer typical of other CC chemokines (Figure 2B). The dimer is predominantly stabilized by interactions between residues 7 and 19 of each subunit that fit into complementary grooves (Figures 2C). Other residues that contribute atoms to the subunit interface include Ser-35, Leu-37, Cys-38, Ser-39, Ile-44, Gln-52, and Cys-54. The interface consists of a combination of hydrophobic and polar interactions that include 10 hydrogen bonds. Approximately 850 Å^2 are buried upon formation of a dimer from the two monomers. The different quaternary structures between the solution and crystal forms

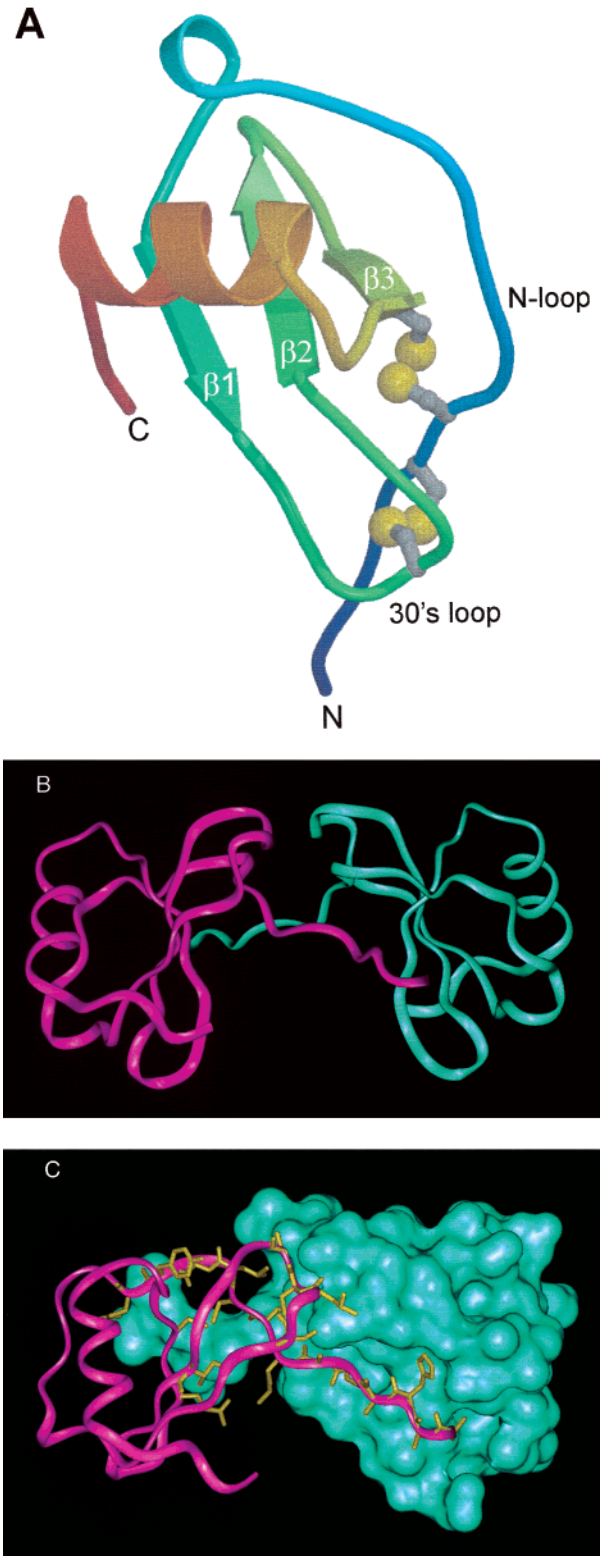

FIGURE 2: (A) Cα trace of the vMIP-II monomer. The disulfide forming cysteine residues are displayed as ball-and-stick models. (B) Dimeric structure of vMIP-II, with each subunit colored green or purple. (C) Subunit interface of the vMIP-II dimer. The solvent-accessible surface of one subunit (in green) shows the groove into which the second subunit (shown in ribbon form) fits. The residues that have atoms within 3.5 Å of the adjacent subunit are also displayed.

of vMIP-II correspond with obvious differences in the monomers. Residues 1−13 in the NMR structure are highly disordered; the subsequent residues (14−19) adopt a different

conformation as compared to the crystal structure of vMIP-II. Leu-46, which in the NMR structure (*37*) protrudes into the surrounding solvent, is closely packed in the crystal structure and contributes to the groove into which the other subunit binds. The factors that promote stabilization of the N-terminus (residues 7−19) and formation of complementary monomer−monomer interactions are not known.

Although significant evidence points toward the chemokine monomer being the active species (*48*, *49*), there is accumulating evidence that the presence of glycosaminoglycans and heparin can induce oligomerization of chemokines (*50*, *51*). However, the physiologically relevant quaternary conformation of chemokines still remains uncertain. We have used the vMIP-II monomer for all subsequent analysis.

Comparison with CCR3-Activating Chemokines. vMIP-II is able to interact with at least eight human chemokine receptors. Our current efforts have focused on understanding the interaction of vMIP-II with CCR3, because interaction with only this receptor leads to signal transduction (*2*). Five other chemokines are agonists for CCR3: eotaxin-1, eotaxin-2, RANTES, MCP-3, and MCP-4 (*52*−*55*). The three-dimensional structures of eotaxin-1 (*56*), RANTES (*57*), and MCP-3 (*58*) have been reported. RANTES is a dimer identical in quaternary structure to vMIP-II. The solution structure of eotaxin-1 is a monomer, but the protein has been shown to exist in monomer−dimer equilibrium. MCP-3 has been reported to be a monomer (*58*) in the structure used here for comparisons. The vMIP-II monomer backbone is very similar in structure to these three chemokines with Cα rms differences of 1.42, 1.53, and 2.20 Å for eotaxin-1, RANTES, and MCP-3, respectively. Superposition of the backbone atoms between the first and last cysteines of eotaxin-1, RANTES, and MCP-3 on vMIP-II is shown in Figure 3A. The largest deviations in backbone conformation of vMIP-II from the other three chemokines are in the N-terminal region. There is also some difference in overlap in the loops between the three β-strands and in the orientation of the C-terminal helix relative to the plane of the β-strands of each chemokine. To gain insight into the structural basis for the binding and activation of CCR3, we compared the surface topology of each protein. We have focused on the N-loop (residues that precede the first β-strand) and the 30s loop, which have been shown to be critical for receptor binding and activation in many chemokines, including RANTES (*21*, *22*, *28*, *49*). Although RANTES and vMIP-II share the greatest degree of identity in amino acid sequence (43%) and backbone structure among the three chemokines, to understand potential interactions with the receptor, it is more appropriate to compare the solvent-exposed molecular surface which involves all accessible atoms in the protein. The molecular surface of the N-loop and the surrounding residues is most similar between eotaxin-1, RANTES, and MCP-3, suggesting a similarity in their interactions with CCR3. The molecular surface of the N-loop region of eotaxin-1, RANTES, and MCP-3 appears as a hydrophobic knoblike protrusion. This apolar region consists of a conserved aromatic residue, which is a phenylalanine in eotaxin-1 and RANTES and a tyrosine in MCP-3 (black circle in Figure 3B). The corresponding region in vMIP-II lacks a similar hydrophobic protrusion, is positively charged, and has the appearance of a groove (white box in Figure 3B). The source of this difference in surface topology is the orientation of the side chain for Leu-16 in vMIP-II, which results in a much smaller occupied volume relative to the aromatic side chains of eotaxin-1, RANTES, and MCP-3. The positive charge in this region of vMIP-II is from residue Lys-40. In eotaxin-1, the corresponding residue is Gln-36, while in RANTES, the corresponding residue is Asn-36 and, therefore, does not contribute to the electrostatics in this region (Figure 4). Although in MCP-3 the corresponding residue is an Arg-38, it is oriented in the opposite direction in the structure and, therefore, does not contribute to the electrostatic potential of the N-loop region. Other notable similarities between eotaxin-1, RANTES, and MCP-3 in this region that are absent in vMIP-II provide further evidence of structural divergence of the viral chemokine. A lysine in the 30s loop, which connects the first and second β-strands, is adjacent to the hydrophobic knob of eotaxin-1 and RANTES and appears as a positively charged protrusion (white circle in Figure 3B). In MCP-3, the corresponding residue is a histidine which also appears as a positive protrusion (white circle in Figure 3B). This is replaced by a leucine residue (Leu-40) in vMIP-II (arrow in Figure 3B). This difference may be particularly important because (1) the 30s loop has been implicated in receptor binding of chemokines (*21*, *22*, *28*, *49*) and (2) electrostatic interactions play an important role in the activation of CCR3 by eotaxin-1 (*59*). In this regard, there are a number of other substantial differences in vMIP-II as compared to eotaxin-1, RANTES, and MCP-3. There appears to be a charge transposition in which Asp-60 and Lys-64 of vMIP-II correspond to Lys-56 and Asp-60 of eotaxin-1, Lys-56 and Glu-60 of RANTES, and Lys-58 and Asp-62 of MCP-3.

Adjacent to the presumed receptor-binding hydrophobic protrusion in eotaxin-1, RANTES, and MCP-3 is a region whose surface topology is that of an apolar groove (boxed in eotaxin-1, RANTES, and MCP-3, Figure 3B). In vMIP-II, this region is also a groove but has a positive potential (black box in Figure 3B). This positive charge is due predominantly to the exposed side chain atoms of Lys-13; in eotaxin-1 and MCP-3, the corresponding residue is a threonine, while in RANTES, the residue is a proline.

The N-terminus of chemokines is known from truncation and site-specific mutagenesis studies to be important for signaling (*22*, *60*, *61*). In most three-dimensional structures of chemokines, however, this N-terminal region is structurally flexible relative to the remainder of the protein (*61*). It appears that a degree of flexibility in the chemokine N-terminus is necessary for making the proper interactions with the receptor, thus leading to signaling. The specific sequence of the N-terminus among various chemokines can reveal properties that are essential for signaling. For example, CXCR1- and CXCR2-activating chemokines require the ELR sequence motif in the N-terminus (*62*). In CCR3 signaling mediated by eotaxin-1, RANTES, and MCP-3, Pro-2 appears to be particularly important (*22*, *63*). In contrast, for vMIP-II there is no proline in the first seven residues of the sequence. Moreover, the N-terminus of eotaxin-1, RANTES, and MCP-3 is largely composed of residues with apolar side chains. Conversely, the vMIP-II N-terminus includes a relatively large number of charged residues. Also, while all the N-terminal residues of eotaxin-1, RANTES, and MCP-3 preceding the first cysteine have small side chains, the N-terminus of vMIP-II includes residues with bulkier side

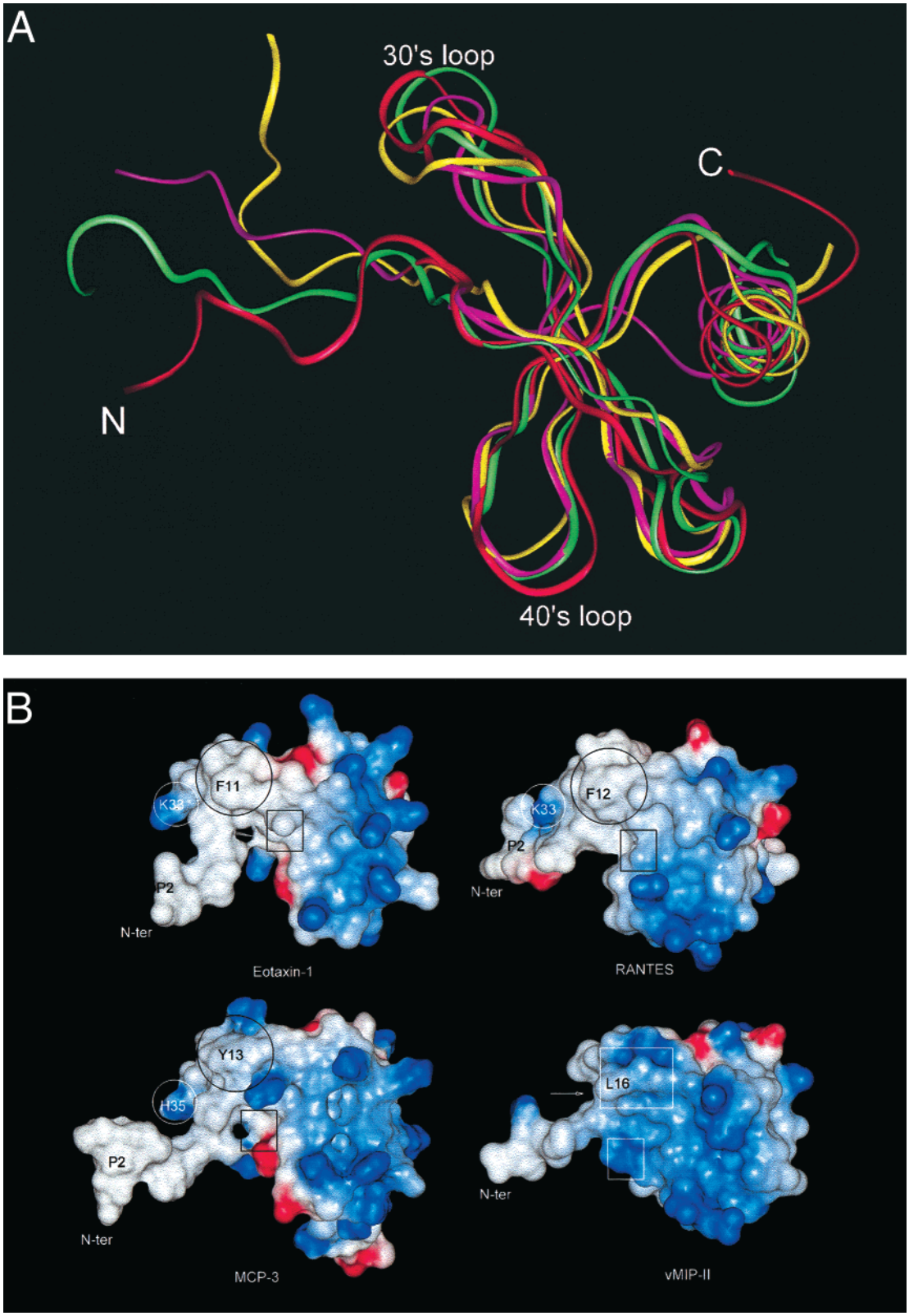

FIGURE 3: (A) Ribbon diagram tracing of the superimposed backbone atoms of eotaxin-1 (red), RANTES (yellow), MCP-3 (green), and vMIP-II (purple). (B) Comparison of surface topologies and electrostatic potentials of eotaxin-1, RANTES, MCP-3, and vMIP-II. The orientation of the four proteins is the same. The N-loop region of eotaxin-1 (F11), RANTES (F12), and MCP-3 (Y13) has the topology of a bulging hydrophobic surface (black circle). The corresponding region of vMIP-II (white box) has the appearance of a positively charged crevice. A second receptor-binding region (from the 30s loop) on eotaxin-1, RANTES, and MCP-3 is the positive knob (K33 in eotaxin-1 and RANTES and H35 in MCP-3) (white circle); in vMIP-II, this region is a groove indicated with the arrow. Below the N-loop bulge is an apolar concave surface in eotaxin-1, RANTES, and MCP-3 (black box). The corresponding region in vMIP-II is positively charged (white box).

chains. Although the significance of these observations remains to be determined, the differences in the sequence between vMIP-II and the CCR3 physiological agonists at the N-terminus are consistent with the structural differences

```
                1
Eotaxin-1:      GP-ASV----PTTCCFNLANRKIPLQRLESYRRITSGK CPQKAVIFKTKLAKDI CADPKKKWVQDSMKYLDQKSPTPKP

                1
RANTES:         SPYSSD----TTPCCFAYIARPLPRAHIKEYFY-TSGK CSNPAVVFVTRKNRQV CANPEKKWVREYINSLEMS------

                1
MCP-3:          QP-VGINT- STTCCYRFINKKIPKQRLESYRRTTSSH CPREAVIFKTKLDKEI CADPTQKWVQDFMKHLDKKTQTPKL

                1
vMIP-II:        GDTLGASWHRPDKCCLGYQKRPLPQVLLSSWYP-TSQL CSKPGVIFLTKRGRQV CADKSKDWVKKLMQQLPVTAR----
```

FIGURE 4: Multiple-sequence alignment of eotaxin-1, RANTES, MCP-3, and vMIP-II. The numbering schemes for eotaxin-1, RANTES, and MCP-3 are identical to those given in entries 1EOT, 1RTO, and 1BO0, respectively. The displayed sequence corresponds to the mature form of vMIP-II corresponding to the protein used by Boshoff et al. (*2*). The alignment was performed using the program DALIGN2 (*71*).

on the N-loop of these chemokines. This suggests that vMIP-II has a novel mode of binding to and activation of the receptor CCR3.

DISCUSSION

vMIP-II possesses the unique capacity to bind a range of receptors that breaches the subfamily specificities established for mammalian chemokines. It is an antagonist for CCR1, CCR2, CCR5, CXCR4 (*3*), CX3CR1 (*4*), and GPR5/XCR1 (*7*); an agonist for CCR3 (*2*); either an agonist or antagonist for CCR8 (*6*, *8*, *9*); and an inverse agonist for the human herpesvirus-8 chemokine receptor (ORF 74) (*64*). The mechanism by which a single chemokine can interact with so many receptors and have different functional effects has only recently begun to be investigated (*65*, *66*). Here we report the crystal structure of vMIP-II and compare it with three physiological CCR3 agonists: eotaxin-1, RANTES, and MCP-3. Our analysis of the vMIP-II surface topology suggests that this viral chemokine employs a unique set of interactions with CCR3. The unique mechanism of vMIP-II may be due to the diverse functional effects (agonism, antagonism, and partial agonism) mediated by promiscuous receptor binding. These effects presumably enhance survival, replication, or transmission of KSHV.

Current evidence supports a two-site model for chemokine−receptor interactions (*60*). A similar model has been proposed for the interactions between C5a and its receptor, except that the receptor binding site consists of regions in the core of C5a and the second site results from the unstructured C-terminus (*67*). In chemokines, sequences in the N-loop, which comprise residues between the two amino-proximal cysteine residues and the first β-strand, confer specificity for receptor binding. Once the chemokine is correctly positioned on the receptor, the residues in the N-terminal segment are utilized for triggering signal transduction. Structural comparisons of vMIP-II and three physiologic ligands of CCR3, eotaxin-1, RANTES, and MCP-3 revealed unexpected differences. All four chemokines have similar degrees of pairwise homology (37−43% identity) and similar numbers of identical residues within the N-loop. Structurally, the largest deviations are in the N-terminus, which in chemokines is known to be flexible and to assume multiple conformations in the unbound state. Similarly, the loops that connect the three β-strands and the C-terminal helix are observed to be flexible in most chemokines. While chemokines of all subfamilies have similar backbone conformations, they display different receptor specificities. The basis of this molecular recognition is a consequence of matching complementary surfaces between the chemokine and its receptor. Since CCR3 responds to eotaxin-1, RANTES, MCP-3, and vMIP-II, we have compared the surface topology and the associated electrostatic potential of these chemokines. If it is assumed that CCR3 binds to these chemokines through the same surface subsections, it may be expected that eotaxin-1, RANTES, MCP-3, and vMIP-II would interact with CCR3 with similar surface topologies. The surface properties of the N-loop for eotaxin-1, RANTES, and MCP-3 are very similar to each other. This region of the N-loop of RANTES has been shown, by site-directed mutagenesis, to direct CCR3 recognition and binding (*22*). In contrast, the surface topology and electrostatic potential of the N-loop for vMIP-II are very different from the corresponding region of eotaxin-1, RANTES, and MCP-3. The surface topology of eotaxin-1, RANTES, and MCP-3 in the N-loop region takes the form of a hydrophobic knob. This apolar bulge in RANTES is due to Phe-12 (Phe-11 in eotaxin-1 and Tyr-13 in MCP-3) and is not observed in the surface topology of vMIP-II in this region. It is likely that this represents a critical difference because only the F12A point mutant was found to lack the ability to bind CCR3 among alanine-scanning mutants of RANTES (*22*). This indicates the importance of the apolar aromatic side chain in making interactions with CCR3. In addition to topological features of the chemokines, which are expected to complement the surface of CCR3, electrostatic interactions have been shown to be important in the activation of CCR3 in response to eotaxin-1 and presumably other agonists (*59*). In this regard, the electrostatic potentials of the N-loop and the surrounding regions of eotaxin-1, RANTES, and MCP-3 are more similar to each other than to vMIP-II. Moreover, comparison of the primary sequence of the N-terminal residues of these chemokines reveals a cluster of basic residues for vMIP-II, some with bulky side chains, but no charged residues for eotaxin-1 and MCP-3, and one aspartic acid for RANTES (Figure 4). Studies of physiological agonists of CCR3, including eotaxin-1, eotaxin-2, and RANTES, confirm the involvement of the N-terminal segment in receptor activation. Cleavage of two N-terminal

residues of eotaxin-1 and RANTES by the protease CD26 was reported to result in proteins that bind CCR3 but lack the ability to induce signaling (*26*, *68*). Similarly, it was found that truncation of three residues of eotaxin-2 (*27*) and alanine-scanning mutagenesis of Pro-2 and Tyr-3 in RANTES eliminated CCR3 agonist activity (*22*). The second residue for eotaxin-1, eotaxin-2, RANTES, and MCP-3 is a proline, a structurally constrained amino acid. The structural significance of this proline residue in the CCR3 signaling mechanism remains to be determined. In contrast, the equivalent position in vMIP-II is occupied by a glycine residue which is structurally the most flexible amino acid. These sequence and structural differences at the N-terminus and N-loop suggest that vMIP-II may have a different mechanism of receptor binding and activation than the physiologic agonists of CCR3. It is likely that vMIP-II employs alternate surface areas for interactions with CCR3. Alternatively, while vMIP-II may continue to make use of the surface topology dictated by the N-loop for binding to CCR3, it might bind to the receptor at a unique but overlapping site also used by eotaxin-1, RANTES, and MCP-3.

It may be expected that chemokines that activate the same receptor do so with similar surface subsections. However, RANTES and MCP-3 also activate other distinct receptors (*61*). When this is taken into account, the similarity in the regions of the surfaces of eotaxin-1, RANTES, and MCP-3 is surprising. We have observed that vMIP-II is the only CCR3 agonist that possesses a surface topology that is different from the physiological agonists, particularly in the presumed receptor-binding site. Also, unlike the other CCR3 agonists (eotaxin-1, RANTES, and MCP-3), vMIP-II does not appear to utilize key residues associated with these physiological agonists in the same manner for CCR3 activation. It is likely that the vMIP-II gene was originally pirated from a mammalian gene and retained the receptor binding properties of the mammalian gene product. The N-loop of vMIP-II is probably involved in interactions with the receptor (or its closest present ancestor) of the original mammalian gene product. During the course of evolution, vMIP-II acquired new properties that conferred benefits to the Kaposi's sarcoma-associated herpesvirus. One possibility may be that vMIP-II was unable to accommodate within the N-loop the selective pressures that resulted in promiscuous receptor binding and diverse functional effects (antagonism, agonism, and inverse agonism) mediated by these receptors. Therefore, new regions of the protein surface were recruited for chemokine receptor interactions with CCR3.

ACKNOWLEDGMENT

We thank Paul Pepin (Yale University), Jimin Wang (Yale University), Paul Adams (Yale University), Marc Deller (Yale University), Phil Evans (Cambridge University, Cambridge, U.K.), and Craig Ogata (Brookhaven National Laboratory) for technical assistance and useful conversations.

REFERENCES

1. Russo, J. J., Bohenzky, R. A., Chien, M. C., Chen, J., Yan, M., Maddalena, D., Parry, J. P., Peruzzi, D., Edelman, I. S., Chang, Y., and Moore, P. S. (1996) *Proc. Natl. Acad. Sci. U.S.A. 93*, 14862−7.
2. Boshoff, C., Endo, Y., Collins, P. D., Takeuchi, Y., Reeves, J. D., Schweickart, V. L., Siani, M. A., Sasaki, T., Williams, T. J., Gray, P. W., Moore, P. S., Chang, Y., and Weiss, R. A. (1997) *Science 278*, 290−4.
3. Kledal, T. N., Rosenkilde, M. M., Coulin, F., Simmons, G., Johnsen, A. H., Alouani, S., Power, C. A., Luttichau, H. R., Gerstoft, J., Clapham, P. R., Clark-Lewis, I., Wells, T. N. C., and Schwartz, T. W. (1997) *Science 277*, 1656−9.
4. Chen, S., Bacon, K. B., Li, L., Garcia, G. E., Xia, Y., Lo, D., Thompson, D. A., Siani, M. A., Yamamoto, T., Harrison, J. K., and Feng, L. (1998) *J. Exp. Med. 188*, 193−8.
5. Sozzani, S., Luini, W., Bianchi, G., Allavena, P., Wells, T. N., Napolitano, M., Bernardini, G., Vecchi, A., D'Ambrosio, D., Mazzeo, D., Sinigaglia, F., Santoni, A., Maggi, E., Romagnani, S., and Mantovani, A. (1998) *Blood 92*, 4036−9.
6. Endres, M. J., Garlisi, C. G., Xiao, H., Shan, L., and Hedrick, J. A. (1999) *J. Exp. Med. 189*, 1993−8.
7. Shan, L., Qiao, X., Oldham, E., Catron, D., Kaminski, H., Lundell, D., Zlotnik, A., Gustafson, E., and Hedrick, J. A. (2000) *Protein Sci. 268*, 938−41.
8. Dairaghi, D. J., Fan, R. A., McMaster, B. E., Hanley, M. R., and Schall, T. J. (1999) *J. Biol. Chem. 274*, 21569−74.
9. Luttichau, B. H., Stine, J., Boesen, T. P., Johnsen, A. H., Chantry, D., Gerstoft, J., and Schwartz, T. W. (2000) *J. Exp. Med. 191*, 171−80.
10. Soulier, J., Grollet, L., Oksenhendler, E., Cacoub, P., Cazals-Hatem, D., Babinet, P., d'Agay, M. F., Clauvel, J. P., Raphael, M., and Degos, L. (1995) *Blood 86*, 1276−80.
11. Navia, B. A., Jordan, B. D., and Price, R. W. (1986) *Ann. Neurol. 19*, 517−24.
12. Liestael, K., Goplen, A. K., Dunlop, O., Bruun, J. N., and Maehlen, J. (1998) *Science 280*, 361−2.
13. Shi, B., De Girolami, U., He, J., Wang, S., Lorenzo, A., Busciglio, J., and Gabuzda, D. (1999) *J. Clin. Invest. 98*, 1979−90.
14. Meucci, O., Fatatis, A., Simen, A. A., Bushell, T. J., Gray, P. W., and Miller, R. J. (1998) *Proc. Natl. Acad. Sci. U.S.A. 95*, 14500−5.
15. Ohagen, A., Ghosh, S., He, J., Huang, K., Chen, Y., Yuan, M., Osathanondh, R., Gartner, S., Shi, B., Shaw, G., and Gabuzda, D. (1999) *J. Virol. 73*, 897−906.
16. Zheng, J., Thylin, M. R., Ghorpade, A., Xiong, H., Persidsky, Y., Cotter, R., Niemann, D., Che, M., Zeng, Y. C., Gelbard, H. A., Shepard, R. B., Swartz, J. M., and Gendelman, H. E. (1999) *J. Neuroimmun. 98*, 185−200.
17. Littman, D. R. (1998) *Cell 93*, 677−80.
18. Berger, E. A., Murphy, P. M., and Farber, J. M. (1999) *Annu. Rev. Immunol. 17*, 657−700.
19. Clark-Lewis, I., Schumacher, C., Baggiolini, M., and Moser, B. (1991) *J. Biol. Chem. 266*, 23128−34.
20. Hebert, C. A., Vitangcol, R. V., and Baker, J. B. (1991) *J. Biol. Chem. 266*, 18989−94.
21. Williams, G., Borkakoti, N., Bottomley, G. A., Cowan, I., Fallowfield, A. G., Jones, P. S., Kirtland, S. J., Price, G. J., and Price, L. (1996) *J. Biol. Chem. 271*, 9579−86.
22. Pakianathan, D. R., Kuta, E. G., Artis, D. R., Skelton, N. J., and Hebert, C. A. (1997) *Biochemistry 36*, 9642−8.
23. Zhang, Y. J., Rutledge, B. J., and Rollins, B. J. (1994) *J. Biol. Chem. 269*, 15918−24.
24. Van Coillie, E., Proost, P., Van Aelst, I., Struyf, S., Polfliet, M., De Meester, I., Harvey, D. J., Van Damme, J., and Opdenakker, G. (1998) *Biochemistry 37*, 12672−80.
25. Gong, J. H., Uguccioni, M., Dewald, B., Baggiolini, M., and Clark-Lewis, I. (1996) *J. Biol. Chem. 271*, 10521−7.
26. Struyf, S., Proost, P., Schols, D., De Clercq, E., Opdenakker, G., Lenaerts, J. P., Detheux, M., Parmentier, M., De Meester, I., Scharpe, S., and Van Damme, J. (1999) *J. Immunol. 162*, 4903−9.
27. Salcedo, T. W., Nardelli, B., Sanyal, I., Olsen, H., Morris, T., Yao, X.-T., Bong, G. W., Zukauskas, D., Kim, Y., Brewer, I., Garotta, G., and Freider, B. (1999) *FASEB J. 13*, A317.
28. Jerva, L. F., Sullivan, G., and Lolis, E. (1997) *Protein Sci. 6*, 1643−52.
29. Daly, T. J., LaRosa, G. J., Dolich, S., Maione, T. E., Cooper, S., and Broxmeyer, H. E. (1995) *J. Biol. Chem. 270*, 23282−92.

30. Proost, P., Struyf, S., Schols, D., Opdenakker, G., Sozzani, S., Allavena, P., Mantovani, A., Augustyns, K., Bal, G., Haemers, A., Lambeir, A. M., Scharpe, S., Van Damme, J., and De Meester, I. (1999) *J. Biol. Chem. 274*, 3988−93.
31. Crump, M. P., Gong, J. H., Loetscher, P., Rajarathnam, K., Amara, A., Arenzana-Seisdedos, F., Virelizier, J. L., Baggiolini, M., Sykes, B. D., and Clark-Lewis, I. (1997) *EMBO J. 16*, 6996−7007.
32. Clark-Lewis, I., Dewald, B., Geiser, T., Moser, B., and Baggiolini, M. (1993) *Proc. Natl. Acad. Sci. U.S.A. 90*, 3574−7.
33. Clark-Lewis, I., Dewald, B., Loetscher, M., Moser, B., and Baggiolini, M. (1994) *J. Biol. Chem. 269*, 16075−81.
34. Mayo, K. H., Roongta, V., Ilyina, E., Milius, R., Barker, S., Quinlan, C., La Rosa, G., and Daly, T. J. (1995) *Biochemistry 34*, 11399−409.
35. Lowman, H. B., Slagle, P. H., DeForge, L. E., Wirth, C. M., Gillece-Castro, B. L., Bourell, J. H., and Fairbrother, W. J. (1996) *J. Biol. Chem. 271*, 14344−52.
36. Shao, W., Fernandez, E., Wilken, J., Thompson, D. A., Siani, M. A., West, J., Lolis, E., and Schweitzer, B. I. (1998) *FEBS Lett. 441*, 77−82.
37. LiWang, A. C., Cao, J. J., Zheng, H., Lu, Z., Peiper, S. C., and LiWang, P. J. (1999) *Biochemistry 38*, 442−53.
38. Dawson, P. E. (1997) *Methods Enzymol. 287*, 34−45.
39. Fernandez, E. J., Joachimiak, A., and Lolis, E. (2000) *J. Appl. Crystallogr. 33*, 168−71.
40. Furey, W., and Swaminathan, S. (1997) *Methods in Enzymology*, Vol. 227, Chapter 31, Academic, San Diego.
41. Terwilliger, T. C., and Berendzen, J. (1999) *Acta Crystallogr. D55*, 849−61.
42. Dodson, E. J., Winn, M., and Ralph, A. (1997) *Methods Enzymol. 277*, 620−33.
43. Collaborative Computational Project 4 (1994) *Acta Crystallogr. D50*, 760−3.
44. de La Fortelle, E., and Bricogne, G. (1997) *Methods Enzymol. 276*, 472−94.
45. Brunger, A. T., Adams, P. D., Clore, G. M., DeLano, W. L., Gros, P., Grosse-Kunstleve, R. W., Jiang, J. S., Kuszewski, J., Nilges, M., Pannu, N. S., Read, R. J., Rice, L. M., Simonson, T., and Warren, G. L. (1998) *Acta Crystallogr. D54*, 905−21.
46. Jones, T. A., Zou, J. Y., Cowan, S. W., and Kjeldgaard, M. (1991) *Acta Crystallogr. A47*, 110−9.
47. Honig, B., and Nicholls, A. (1995) *Science 268*, 1144−9.
48. Rajarathnam, K., Sykes, B. D., Kay, C. M., Dewald, B., Geiser, T., Baggiolini, M., and Clark-Lewis, I. (1994) *Science 264*, 90−2.
49. Mizoue, L. S., Bazan, J. F., Johnson, E. C., and Handel, T. M. (1999) *Biochemistry 38*, 1402−14.
50. Hoogewerf, A. J., Kuschert, G. S., Proudfoot, A. E., Borlat, F., Clark-Lewis, I., Power, C. A., and Wells, T. N. (1997) *Biochemistry 36*, 13570−8.
51. Kuschert, G. S., Coulin, F., Power, C. A., Proudfoot, A. E., Hubbard, R. E., Hoogewerf, A. J., and Wells, T. N. (1999) *Biochemistry 38*, 12959−68.
52. Daugherty, B. L., Siciliano, S. J., DeMartino, J. A., Malkowitz, L., Sirotina, A., and Springer, M. S. (1996) *J. Exp. Med. 183*, 2349−54.
53. Uguccioni, M., Loetscher, P., Forssmann, U., Dewald, B., Li, H., Lima, S. H., Li, Y., Kreider, B., Garotta, G., Thelen, M., and Baggiolini, M. (1996) *J. Exp. Med. 183*, 2379−84.
54. Ponath, P. D., Qin, S., Post, T. W., Wang, J., Wu, L., Gerard, N. P., Newman, W., Gerard, C., and Mackay, C. R. (1996) *J. Exp. Med. 183*, 2437−48.
55. Forssmann, U., Uguccioni, M., Loetscher, P., Dahinden, C. A., Langen, H., Thelen, M., and Baggiolini, M. (1997) *J. Exp. Med. 185*, 2171−6.
56. Crump, M. P., Rajarathnam, K., Kim, K. S., Clark-Lewis, I., and Sykes, B. D. (1998) *J. Biol. Chem. 273*, 22471−9.
57. Chung, C., Cooke, R., Proudfoot, A., and Wells, T. (1995) *Biochemistry 34*, 9307−14.
58. Kim, K. S., Rajarathnam, K., Clark-Lewis, I., and Sykes, B. D. (1996) *FEBS Lett. 395*, 277−82.
59. Dairaghi, D. J., Oldham, E. R., Bacon, K. B., and Schall, T. J. (1997) *J. Biol. Chem. 272*, 28206−9.
60. Monteclaro, F. S., and Charo, I. F. (1996) *J. Biol. Chem. 271*, 19084−92.
61. Baggiolini, M., Dewald, B., and Moser, B. (1997) *Annu. Rev. Immunol. 15*, 675−705.
62. Rollins, B. J. (1997) *Blood 90*, 909−28.
63. Ponath, P. D., Qin, S., Ringler, D. J., Clark-Lewis, I., Wang, J., Kassam, N., Smith, H., Shi, X., Gonzalo, J. A., Newman, W., Gutierrez-Ramos, J. C., and Mackay, C. R. (1996) *J. Clin. Invest. 97*, 604−12.
64. Geras-Raaka, E., Varma, A., Clark-Lewis, I., and Gershengorn, M. C. (1998) *Biochem. Biophys. Res. Commun. 253*, 725−7.
65. Liwang, A. C., Wang, Z. X., Sun, Y., Peiper, S. C., and Liwang, P. J. (1999) *Protein Sci. 8*, 2270−80.
66. Zhou, N., Luo, Z., Luo, J., Hall, J. W., and Huang, Z. (2000) *Biochemistry 39*, 3782−7.
67. Siciliano, S. J., Rollins, T. E., DeMartino, J., Konteatis, Z., Malkowitz, L., Van Riper, G., Bondy, S., Rosen, H., and Springer, M. S. (1994) *Proc. Natl. Acad. Sci. U.S.A. 91*, 1214−8.
68. Oravecz, T., Pall, M., Roderiquez, G., Gorrell, M. D., Ditto, M., Nguyen, N. Y., Boykins, R., Unsworth, E., and Norcross, M. A. (1997) *J. Exp. Med. 186*, 1865−72.
69. Esnouf, R. M. (1997) *J. Mol. Graphics Modell. 15*, 132−4.
70. Merritt, E. A., and Bacon, D. J. (1997) *Methods Enzymol. 277*, 505−24.
71. Morgenstern, B. (1999) *Bioinformatics 15*, 211−8.
72. Esnouf, R. M. (1997) *J. Mol. Graphics Modell. 15*, 112−3.

BI001166F